

# Ultra-discrete kinks with supersonic speed in a crystal with realistic potentials

J. F. R. Archilla,<sup>1</sup> Y. A. Kosevich,<sup>2</sup> N. Jiménez,<sup>3</sup> V. Sánchez-Morcillo,<sup>3</sup> and L. M. García-Raffi<sup>4</sup>

<sup>1</sup>*Grupo de Física No Lineal. Universidad de Sevilla. ETSI Informática, Avda Reina Mercedes s/n, 41012-Sevilla, Spain*

<sup>2</sup>*Semenov Institute of Chemical Physics, Russian Academy of Sciences. Ul. Kosygina 4, 119991 Moscow, Russia*

<sup>3</sup>*Instituto de Investigación para la Gestión, Integrada de las Zonas Costeras, Universidad Politécnica de Valencia, C/.Paraninfo 1, 46730 Grao de Gandia, Spain*

<sup>4</sup>*Instituto Universitario de Matemática Pura y Aplicada, Universidad Politécnica de Valencia, Camino de Vera s/n, 46022 Valencia, Spain*

We have progressively developed a simplified model of the cation layer in a silicate, starting from purely electrostatic repulsion, adding short range repulsive potential and afterwards a periodic potential due to the other atoms of the lattice. A simple method allows the production of supersonic kinks which propagate in the lattice with a large range of energies and velocities. The introduction of the lattice potential brings about that the kinks propagate with a single velocity and energy, independent of the excitation. The kinks found are supersonic and ultra discrete, only two or one particle are moving at a given time. This discreteness allow the explanation of the double kink also found in other supersonic systems. The energy of the lattice kinks is in agreement with the fossil and experimental evidence of localized transmission of energy in silicates between the energy given by  $^{40}\text{K}$  recoil and the sputtering energies.

PACS numbers: 63.20.Pw, 63.20.Ry, 05.45.-a

Keywords: kinks, crowdion, silicates, mica, muscovite, ILMs, breathers

## I. INTRODUCTION

Many minerals are known by their capability of recording the tracks of charged particles, and are often used as solid state nuclear track detectors (SSNTDs); a review of the subject can be found in Refs.<sup>1,2</sup>. One of such minerals is mica muscovite, for which tracks of positrons, muons and other particles have been reported<sup>3-6</sup>. Some of these tracks were identified as produced by positrons resulting from the  $\beta^+$  decay of  $^{40}\text{K}$ . This isotope is relatively abundant in the mineral and can also experience  $\beta^-$ , electron capture and other kind of decays as explained in the appendix. Most of the tracks, however, could not be explained by charged particles but could have been produced by some kind of vibrational excitation because, among other properties, the tracks are along the close-packed lines of the  $\text{K}^+$  hexagonal layer shown in Fig. 1. One interpretation of these tracks is that they are formed by localized, nonlinear excitations, sometimes called *quodons*<sup>7</sup>, whose exact nature is still not known.

A likely source for the vibrational energy required to initiate a quodon is the recoil of  $^{40}\text{K}$  after  $\beta$  decay, which can be between 8 and 52 eV as explained in the appendix. In muscovite, there are about 3 decays per second and  $\text{cm}^3$ , so after many years of the sensitive period, when tracks recording is possible, there are many possibilities to initiate a quodon. An experiment was done to shed some light into the relationship between tracks and quodons<sup>8</sup>. A mica specimen was irradiated with alpha particles and the ejection of atoms was detected at the other side, along closed packed lines. The ejected atoms could not be identified and also sputtering energies are not known exactly, however from experimental and theoretical studies they are known to be on the range of

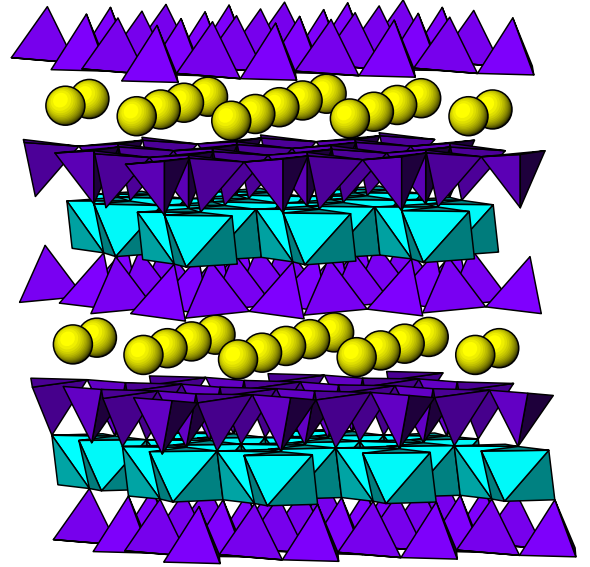


FIG. 1: Representation of the mica structure with a point of view that emphasizes the close-packed lines of  $\text{K}^+$  represented by yellow balls. For a view from the top see Fig. 10

4-8 eV<sup>9</sup>.

In an attempt to understand this phenomenon, numerical simulations were conducted in an idealized 1D model where particles of increasing energy hit the boundary of the lattice<sup>10</sup>. The study reports the formation of breather and kinks and the ejection of atoms at the opposite boundary of the sample. However, the model did not intend to use realistic values of the mica muscovite parameters.

A minimal model of the cation lattice with realistic parameters was proposed recently<sup>11,12</sup>. Only  $\text{K}^+$  ions were

considered with the actual potassium mass and Coulomb interaction between them. The interaction with the rest of the lattice was implicitly considered as the force keeping the ions inside the crystal with the interatomic distance in muscovite. In those publications, it was reported the existence of supersonic kinks, which were very easily generated with a large range of energies and velocities.

However such model was too simplistic as for relatively high energies the minimal distances between ions of tenths of angstrom was not realistic. Therefore, in the present work we introduce a short range interaction used in particle bombardment studies<sup>13</sup>. It corresponds to the Coulomb repulsion between nuclei (not ions) partially screened by the atom electrons. It decays rapidly in a few Å. The results are similar to those obtained with only Coulomb interaction<sup>11,12</sup>, i.e., supersonic kinks that travel without dispersion can be produced with arbitrary energies, but now the inter-particle distances are limited to physically reasonable values. Note that our model allows for bond dissociation, which is a necessary condition for realistic results as finite thermal conductivity<sup>14</sup>.

As a next step towards a more realistic description, we construct explicitly the interaction with the surrounding atoms, using standard empiric potentials used in molecular dynamics, giving rise to a periodic non-sinusoidal substrate potential. Supersonic lattice kinks, also called *crowdions*<sup>15</sup>, are also easily obtained, now propagating with a velocity independent of the input, only determined by the lattice parameters. For smaller energies the kink dissipates in phonons, for larger energies the excess energy is radiated until reaching the crowdion's one. The final crowdion energy is approximately 26 eV, which can be provided by the recoil of isotopes of potassium after radioactive decay and are larger than the sputtering energies. This suggest that lattice kinks or crowdions can be related to the tracks found in muscovite.

Literature about kink propagation in lattices with different inter-particle and on-site potentials is extensive. The most studied and generic model is the Frenkel-Kontorova equation (F-K), (see reviews in Refs.<sup>16,17</sup>). However most of the cases considered are subsonic. Supersonic kinks in systems with substrate have been found in models with anharmonic coupling<sup>15,18,19</sup>. They have the property than only a discrete set of velocities allow the propagation of kinks without attenuations. They can be described as multi-kinks or N-solitons depending if the description is done in terms of coordinates, strains or velocities. It is speculated that the multi-kink phenomenon corresponds to some matching between the kink and the lattice unit and/or between the interaction and substrate energies. The unique kink propagating in our model with substrate is also a double-kink.

F-K models have also been considered in layered materials, for example, to model in plane motions of few-layer graphene, in order to explain molecular-dynamics simulation results for cross-plane thermal conductance<sup>20</sup>.

One particular characteristic found in the kinks studied in the present work is their extreme discreteness, i.e.,

only two particles and for higher energies almost only one particle is in motion at a given time. This discreteness allow the complete understanding in physical terms of the mechanism that brings about a single velocity and why it is a double kink.

The paper is organized as follows, first we review and extend the results obtained with only Coulomb interaction, using the sinusoidal waveform proposed for supersonic kinks in FPU systems<sup>21</sup>, which is a good description for  $\lambda \simeq 3$  but for  $\lambda \simeq 2$  fails, been replaced by an almost triangular waveform, corresponding to nearly hard spheres collisions. Afterwards we consider interactions with several neighbours and introduce a ZBL short range potential. Thereafter, the substrate potential is constructed and the properties of the single-velocity lattice kinks are analyzed with detail.

## II. MODEL AND SINUSOIDAL KINK DESCRIPTION

We consider as a starting point a one-dimensional minimal model for the dynamics of  $K^+$  ions, given in dimensionless form by

$$\ddot{u}_n = -\frac{1}{(1+u_{n+1}-u_n)^2} + \frac{1}{(1+u_n-u_{n-1})^2}. \quad (1)$$

which describes a chain of ions coupled to their nearest neighbours by electrostatic potentials. The variables  $u_n$  represent the displacement of a particle in the chain with respect to its equilibrium position, normalized to the lattice constant. The values of the scaled units are: for lengths, the equilibrium distance between  $K^+$  ions,  $a = 5.19$  Å; for masses, the mass of a  $K^+$  ion,  $m_{K^+} = 39.1$  amu; for time  $\tau = \sqrt{m_K a^3 / k_e e^2} \simeq 0.2$  ps, being  $k_e$  the Coulomb constant and  $e$  the elementary unit of charge. Other derived units are velocity  $u_V = 2.6$  km/s, energy  $u_E = 2.77$  eV and frequency 5 THz. The speed of sound in this system is  $c_s = \sqrt{2}$  or 3.7 km/s in physical units.

For small amplitudes, the potentials in Eq. (1) can be expanded in series, using that  $1/(1+y)^2 \simeq 1 - 2y + 3y^2 - 4y^3 \dots$ . Retaining cubic terms and smaller, we obtain:

$$\ddot{u}_n = c_s^2 [(u_{n+1} + u_{n-1} - 2u_n) - 3/2(u_{n+1} - u_n)^2 + 3/2(u_n - u_{n-1})^2 + 2(u_{n+1} - u_n)^3 - 2(u_n - u_{n-1})^3 + \dots]. \quad (2)$$

which is the  $\alpha - \beta$  FPU equation. Neglecting nonlinear terms, it reduces to the discrete linear wave equation,

$$\ddot{u}_n = c_s^2 (u_{n+1} + u_{n-1} - 2u_n) \quad (3)$$

where  $c_s$ , the speed of sound, is the long wavelength phonon velocity. It is also both the maximum phase and group velocity. Note that in our scaling  $c_s = \sqrt{2}$ , while usually it is such that  $c_s = 1$ . The latter is not convenient in our model, because it would introduce a factor

in the dimensionless Coulomb law. We keep in what follows the term  $c_s$  without substitution, both for ease of comparison and because it has an important physical meaning.

Introducing a new variable, the deformation from the equilibrium position or *strain*  $v_n = u_n - u_{n-1}$ , the equations above can be written as:

$$\ddot{v}_n = 2F_n - F_{n+1} - F_{n-1}; \quad \text{with} \quad F_n = \frac{1}{(1 + v_n)^2} \quad (4)$$

$v_n = 0$  corresponding to the unperturbed lattice. The boundary conditions are fixed particles at the ends of the lattice. Kinks are produced numerically by applying at the chain boundary a *half wave* perturbation, that is, a sinusoidal displacement during half a period, starting and finishing at the equilibrium position<sup>11,21</sup>. In order to describe a kink travelling to the right, in Ref.<sup>21</sup> the following *ansatz* was introduced

$$v_n = -\frac{A}{2}(1 + \cos(qn - \omega t)) \quad \text{if} \quad -\pi \leq qn - \omega t < \pi \quad (5)$$

and  $v_n = 0$  otherwise, where  $A$  is the kink amplitude. The bonds are always compressed so  $v_n$  is negative with a minimum value of  $-A$ , corresponding to the maximum compression of the bond. For analogy, we use the usual wave terminology, so  $\phi_n = \omega t - qn$  is the phase;  $q$ , the wave number;  $\omega$ , the angular frequency;  $T$ , the period;  $\lambda = 2\pi/q$ , the wavelength and so on. The sinusoidal description is not an exact solution of the system but it is reasonably accurate for intermediate values of the amplitude  $A$  and it provides a very useful framework to understand the relative phases of the particles and the behaviour of the kink.

Figure 2 (top) compares the result of the numerical simulation for displacements and strains, with the corresponding analytical expressions derived from Eq. (5), for an intermediate value of the amplitude  $A = 0.55$  and wave number  $q \simeq 2\pi/3$ . The analytical expression fits very well the numerical data. Figure 2 (bottom) pictures a kink with wavenumber  $q = \pi$ . There are not enough particles to compare with the analytical form, but the main properties of the latter are valid.

For the wave number  $q = 2\pi/\lambda$ , with  $\lambda$  an integer, Eq. (5) represents a solution where basically  $\lambda$  bonds and  $\lambda - 1$  particles (the kink core) are in motion, while the others remain at rest.

We will use the term *active* to describe related states of the different magnitudes. The active particles or coordinates at a given time or time interval (or phase or phase interval) are those such  $u_n$  is changing, the active bonds are those for which  $v_n \neq 0$ , i.e., the compressed ones. For a particle the active time interval is when it is moving, and for a bond when it is compressed.

If  $\lambda$  is between two integers  $m_1$  and  $m_2$  then the number of active bonds oscillates between  $m_1$  and  $m_2$  and the number of active particles oscillates between  $m_1 - 1$  and  $m_2 - 1$ .

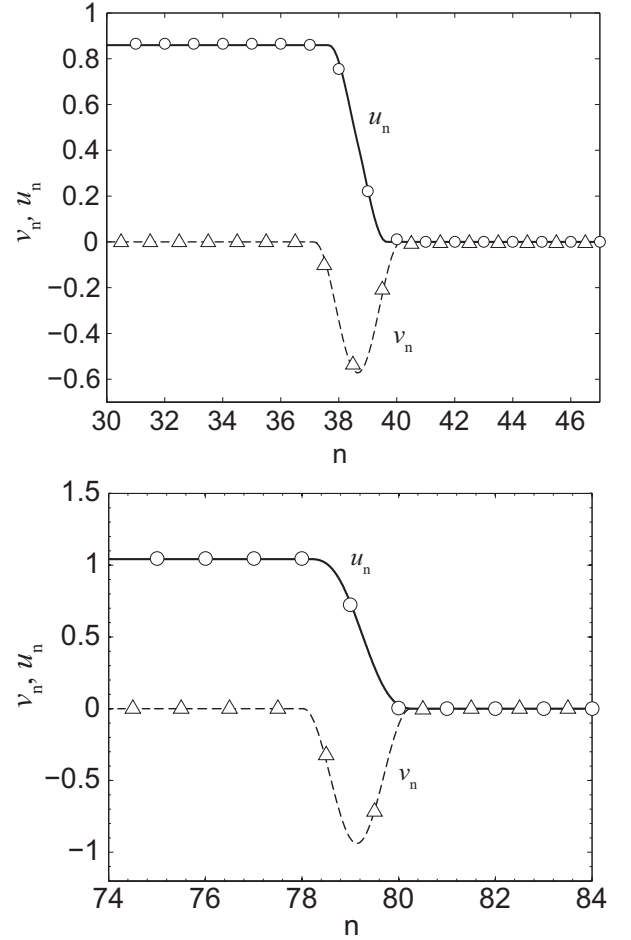


FIG. 2: Profile for the two kinks coordinates  $u_n$  and strains  $v_n = u_n - u_{n-1}$ . Circles and triangles are numerical results and the continuous lines are obtained from Eq. (5) with *magic* wavenumber  $q \simeq 2\pi/3$  (top), where basically two particles are moving at a given time and with  $q \simeq \pi$  (bottom), with amplitude close to 1, where basically one particle is moving at a given time. Scaled units are equal to the lattice unit.

Of particular interest in this work will be  $\lambda = 3$ , for which  $q = 2\pi/3$  is called the *magic wave number* and  $\lambda = 2$ , with  $q = \pi$ , which will be referred simply as the mode  $\pi$ . These two values are extremes cases of localization being  $q = \pi$  the limit, only one particle is moving at a given time.

### Rotating wave approximation

The velocities of the kinks can be analytically obtained using the rotating wave approximation (RWA) as derived in Ref.<sup>11</sup>:

$$V = \frac{\omega}{q} = \frac{1}{(1 - A)^{3/4}} c_s \frac{\sin(q/2)}{q/2}. \quad (6)$$

Kinks are therefore supersonic. For low amplitude ( $A \rightarrow 0$ ) and long wavelength ( $q \rightarrow 0$ ),  $V$  tends to the sound speed  $c_s$ .

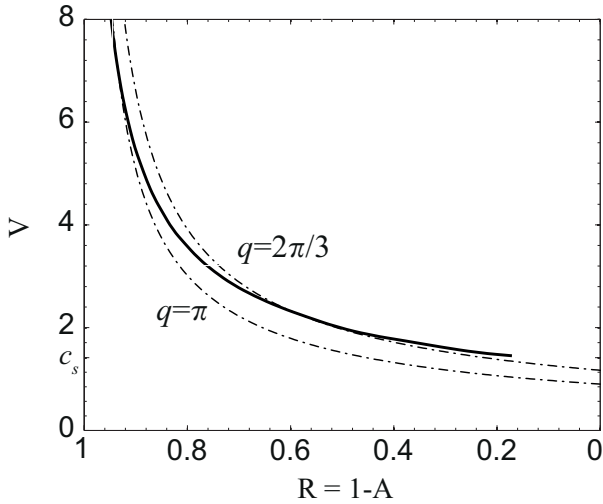


FIG. 3: Kink velocity calculated numerically (thick line), and analytical results from Eq.(6) with wave vector  $q = 2\pi/3$  (upper dotted-dashed line) and  $q = \pi$  (lower dotted-dashed line). Scaled units are the lattice unit for distances and 2.6 km/s for velocities.

In Ref.<sup>11</sup> it was shown that the magic wave number represents a reasonable good agreement between the *ansatz* and the simulations. However this agreement failed at amplitudes  $A$  approaching unity, i.e. the lattice parameter in scaled variables, where  $q = \pi$  brings about a much better fit as can be seen in Fig. 3. The conclusion is that the magic wave number is a suitable approximation for an intermediate range of amplitudes, but that actually  $q$  changes continuously with the amplitude. The complementary approach is to use Eq. (6) to find the values of the wave number  $q$ , with respect to the amplitude  $A$  or the velocity  $V$ . This will be seen in Fig. 8, where it can be appreciated that the magic number is a satisfactory solution only for intermediate values.

### Triangular wave form

At higher amplitudes closer to 1, the waveform deviates from the sinusoidal description of Eq. (5) and approaches instead to a triangular waveform, as shown in Fig. 4. The almost straight lines mean that the velocity is almost constant except during a very short interaction time. The system behaviour is very similar to a hard spheres model.

This waveform is also another way of looking at the mode  $q = \pi$ . In this mode only one particle is moving at a given time, which means that there are no forces with their neighbours, because those forces would accelerate them. Strictly speaking, the mode  $q = \pi$  and an exact

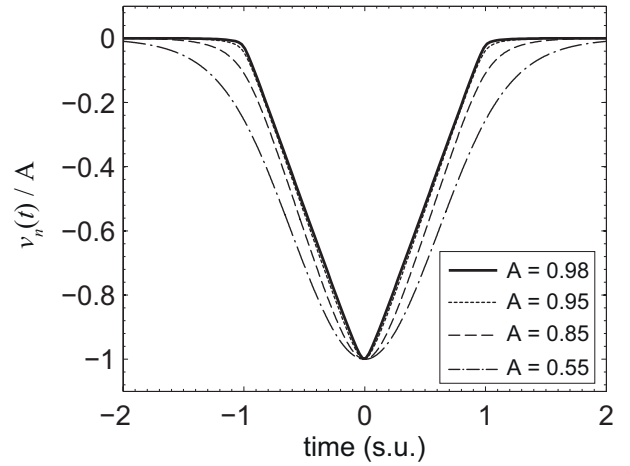


FIG. 4: Temporal variation of the strain  $v_n = u_n - u_{n-1}$  for different amplitudes. As the amplitude  $A$  increases the shape becomes almost triangular, corresponding to almost hard spheres collisions. The amplitude  $A$  is given in lattice units and the scaled time unit is 2 ps.

triangular waveform are unattainable as the electrostatic forces are acting on the particles. However, if the energy of the particles is large with respect to the change in potential during a large part of the path between collisions, the behaviour will be quite similar during much of the path. They have been described as the high-energy limit for Lennard-Jones interatomic potentials<sup>22</sup> and observed experimentally in a system of repelling magnets<sup>23</sup>.

### A. Analytical results

#### 1. Sinusoidal waveform and $q = 2\pi/3$

Some analytical results can be obtained in this model. Let us consider the wavenumber  $q = 2\pi/3$  and choose  $t = 0$  the time for which  $\phi_n = qn - \omega t = 0$  at  $n = 0$  after a change of the origin of  $n$  and  $t$ , but keeping the notation  $n$  for generality. If we consider the time interval  $\Delta t$ :  $-T/6 \leq t < T/6$ , there are three active strains:  $v_{n+1}$ ,  $v_n$  and  $v_{n-1}$ . At the end of the interval, that is at  $t = T/6$ ,  $v_{n-1}$  becomes zero and  $v_{n+2}$  starts being perturbed, so all the indexes  $n$ 's of the particles will change in an unity.

During  $\Delta t$ ,  $u_{n'} = 0$  for  $n' \geq n + 1$ ,  $u_n$  and  $u_{n+1}$  are changing but  $u_{n-1}$  has already attained  $3A/2$  its final constant value as can be checked by direct sum. Also,  $u_{n'} = 3A/2$  for  $n' < n - 1$ , their final value after the kink has passed over them as seen in Fig. 2. The active coordinates are therefore  $u_n = -v_{n+1}$  and  $u_{n-1} = -v_n + v_{n+1}$ . After some manipulation we get

$$\begin{aligned} u_n &= \frac{A}{2} + \frac{A}{2} \cos(\phi_n + 2\pi/3) \\ u_{n-1} &= A - \frac{A}{2} \cos(\phi_n - 2\pi/3). \end{aligned} \quad (7)$$

We can obtain immediately the kink kinetic energy as  $K = \frac{1}{2}\dot{u}_n^2 + \frac{1}{2}\dot{u}_{n-1}^2$ , which results

$$K = \frac{\omega^2 A^2}{8} \left(1 + \frac{1}{2} \cos(2\phi_n)\right). \quad (8)$$

with maximum value

$$K_M = \frac{\pi^2}{12} V^2 A^2. \quad (9)$$

$$(10)$$

The potential energy with respect to the equilibrium state is given by

$$U = \frac{1}{1+v_{n-1}} + \frac{1}{1+v_n} + \frac{1}{1+v_{n+1}} - 3. \quad (11)$$

By substitution, it can be seen that the maximum potential energy corresponds to the bond  $n$  at its maximum compression, i.e., with  $\phi_n = 0$  and while the bonds  $n-1, n+1$  have a phase difference of  $\pm 2\pi/3$  with strain  $u_{n-1, n+1} = -A/2(1 + \cos(\pm 2\pi/3)) = -A/4$ . Therefore the maximum energy becomes:

$$U_M = \frac{1}{1-A} + \frac{2}{1-A/4} - 3. \quad (12)$$

$$(13)$$

There is also a minimum potential energy which corresponds to the limit case where only two bonds are different from zero with phase  $\pm\pi/3$  and strain  $v_n = -3A/4$ . The minimum energy becomes

$$U_m = \frac{2A}{1-3A/4} - 2. \quad (14)$$

$$(15)$$

The kink has always some compression energy  $U_m$  above the ground state.

### 2. Sinusoidal waveform and mode $q = \pi$

The properties of sinusoidal kinks with mode  $q = \pi$  are easy to obtain as there are only two active strain variables and a coordinate one, which during the interval  $\Delta_\pi t$ :  $0 \leq t < T/2$  are

$$\begin{aligned} v_n &= -\frac{A}{2}(1 + \cos(qn - \omega t)); \\ v_{n+1} &= -\frac{A}{2}(1 + \cos(q[n+1] - \omega t)) = \\ &\quad -\frac{A}{2}(1 - \cos(qn - \omega t)); \\ u_n &= -v_{n+1} \quad ; \quad \dot{u}_n = \frac{A}{2}\omega \sin(qn - \omega t) \end{aligned} \quad (16)$$

The kinetic and potential energies  $K = \frac{1}{2}\dot{u}_n^2$  and  $U = \frac{1}{1+v_n} + \frac{1}{1+v_{n+1}} - 2 = \frac{1}{1+v_n} + \frac{1}{1-v_n} - 2$ , can be obtained. The maximum kinetic, maximum and minimum potential energies are given by

$$K_M = \frac{\pi^2}{8} A^2 V^2; \quad U_M = \frac{1}{1-A} - 1; \quad U_m = \frac{2}{1-A/2} - 2 \quad (17)$$

### 3. Triangular waveform and $q = \pi$

The potential energy fits very well the numerical values, unlike the kinetic energy, as can be seen in Figs. 5 and 6. This is because the  $\pi$  kink is better described by a triangular form for large energies. Let us suppose that at  $t = 0$  is the time for which  $v_n = -A$ , as it takes half a period to change from  $-A$  to 0, then  $VT/2 = 2$ . Therefore, for the interval  $0 \leq t < T/2$  the active variables are:

$$\begin{aligned} v_n &= -A + AVt; & v_{n+1} &= -AVt \\ u_n &= -v_{n+1} = AVt; & \dot{u}_n &= AV \end{aligned} \quad (18)$$

The kinetic energy is therefore constant:

$$K = K_M = \frac{1}{2} A^2 V^2, \quad (19)$$

In the numerical simulations, there are short time intervals when  $K$  changes, separated by a larger interval when  $K$  is almost constant.

The maximum and minimum potential energies are identical to the  $q = \pi$  sinusoidal form in Eq. (17)

## III. INTERACTION WITH SEVERAL NEIGHBOURS

All the previous results apply to the case of nearest neighbour coupling. We have also checked that the kinks still exist and propagate supersonically when the Coulomb interaction extends beyond the nearest neighbors. The kinks have similar velocity and wave number if we take as reference a normalized velocity  $V/c_p$ , where  $c_p = c_s \left(\sum_{l=1}^p 1/l\right)^{1/2}$  is the sound speed in the chain with interactions with  $p$  nearest neighbours. Fig. 7 shows the dependence of the relative velocity  $V/c_p$  with the minimum interparticle distance and Fig. 8 shows the dependence of the best fit for the wavenumber as a function of the relative velocity, emphasizing the essential identity of the phenomenon. Other aspects of these figures will be commented below. For clarity, only the cases of three and eight neighbours are represented although up to 30 neighbours have been tested.

It is worth commenting the problem that arises when the interaction with an infinite number of neighbours is taken into account. If the pair potential depends on the



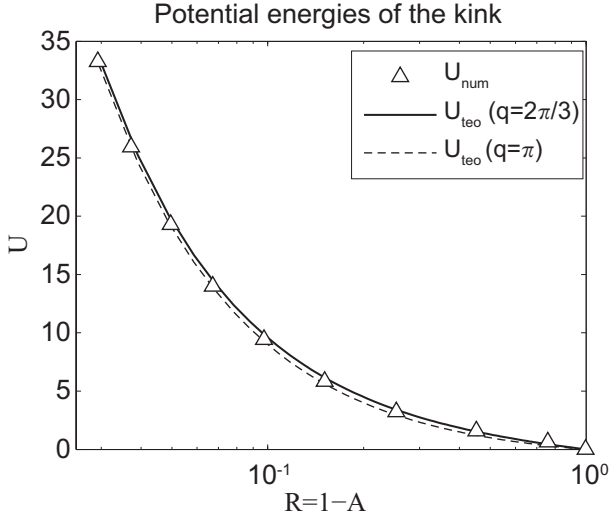


FIG. 5: Maximum potential energies of the kinks with Coulomb potential for amplitudes  $A$  close to 1 (or interparticle distance  $R$  very small). The analytical results are very similar for waveforms  $q = \pi$  or  $q = 2\pi/3$ , as the maximum potential energy of the kink depends mainly of the minimum separation between particles  $R$ . The values of the scaled units are the lattice unit and 2.77 eV respectively.

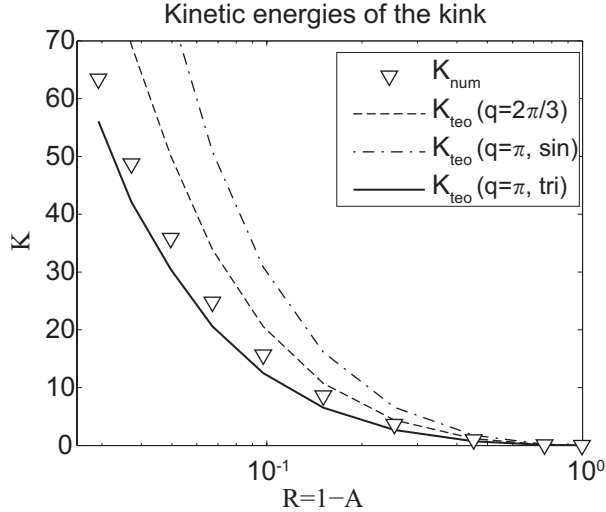


FIG. 6: Maximum kinetic energies of the kinks with Coulomb potential for amplitudes  $A$  close to 1 or interparticle distance  $R$  very small (note the logarithmic scale for  $R$ ). It can be seen that the kink with wavenumber  $\pi$  is better described by a triangular wave form than a sinusoidal one, although not exactly. The values of the scaled units are the lattice unit and 2.77 eV respectively.

interparticle distance  $|r|$  as  $1/|r|^s$ , the long-wave phonon velocity is finite for  $s > 1$ , but it diverges with the number of particles  $N$  as  $v_{ph} \propto \sqrt{\ln(N/2)}$  for the unscreened Coulomb potential ( $s = 1$ ). However, this divergence occurs only in the electrostatic limit where the electromagnetic wave retardation is neglected. With an account

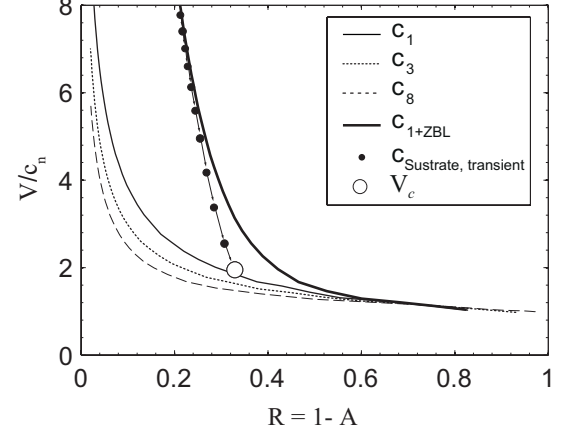


FIG. 7: Kink velocities as a function of minimal distance  $R$  (in lattice units) for several potentials. Key to legend:  $c_i$ : Coulomb interaction between the first  $i$  neighbours. Velocities are normalized to the sound speed  $c_p$  for a system with interaction with  $p$  neighbours, except for the system with substrate which is normalized to  $c_1 = c$ . It can be seen that the increase of the number of neighbours taking into account with Coulomb interaction slows the kink in normalized velocity  $V/c_p$  (but not in absolute velocity). Also, it can be seen that the radiative process in the system with substrate takes it from the curve  $c_{1+ZBL}$  to some specific velocity within the  $c_1$  curve. The values of the sound velocities are  $c_1 = c_s = 3.7$  km/s,  $c_3 = 5.0$  km/s and  $c_8 = 6.1$  km/s.

of the retardation the long-wave group velocity tends to the speed of light in vacuum. If the particles are in a material medium, there is a rearrangement of the electron density that can be described as a screening of the Coulomb interaction with some characteristic length  $l_{scr}$ . The screening brings about a finite long-wave phonon velocity  $v_{ph} \propto \sqrt{\ln(l_{scr}/a)}$ , where  $a$  is the lattice constant. As it has been commented, we do not deal with this important theoretical problem and have considered only a few neighbours for simplicity.

#### IV. KINKS WITH ZBL SHORT-RANGE POTENTIAL

The minimum interatomic distance  $R = 1 - A$  obtained for fast kinks is clearly impossible in realistic systems. At short distances short-range forces appear, they are produced by the overlapping electric states of the two approaching atoms. A large number of different repulsive potentials and screening functions have been proposed over the years, some determined semi-empirically, others from theoretical calculations. A much used repulsive potential is the one given by Ziegler, Biersack and Littmark, the so-called ZBL repulsive potential. It has been constructed by fitting a universal screening function to theoretically obtained potentials calculated for a large

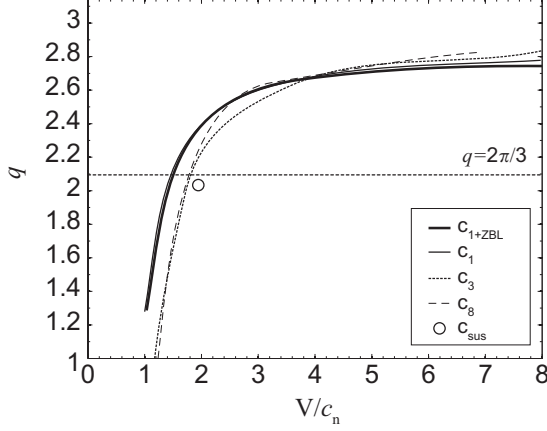


FIG. 8: Best fit of the wavenumber  $q$  of the kinks as a function of the velocities normalized to the sound speed. Key to legend:  $c_i$ : Coulomb interaction between the first  $i$  neighbours. Note that the *magic* wavenumber is also chosen by the system with substrate. The values of the sound velocities are  $c_1 = c_s = 3.7$  km/s,  $c_3 = 5.0$  km/s and  $c_8 = 6.1$  km/s.

variety of atom pairs<sup>13</sup>. The ZBL potential has the form

$$U_{\text{ZBL}}(r) = k_e \frac{Z_1 Z_2 e^2}{r} \phi\left(\frac{r}{\rho}\right), \quad (20)$$

with  $k_e$  being the Coulomb constant,  $Z_1$  and  $Z_2$ , the atomic numbers of the involved atoms, and  $\phi(x)$ , the universal screening function:

$$\phi(x) = 0.1818 \exp(-3.2x) + 0.5099 \exp(-0.9423x) + 0.2802 \exp(-0.4029x) + 0.02817 \exp(-0.2016x) \quad (21)$$

Here  $Z_1$  and  $Z_2$  are the atomic numbers of the interacting nuclei, and  $r$  the distance between them. The screening length is  $\rho = 0.8854 a_0 / (Z_1^{0.23} + Z_2^{0.23})$ , being  $a_0 = 0.529$  the Bohr radius. The ZBL potential describes well the interaction between neutral atoms. In the case of ions considered here, the Coulomb potential must also be added, accounting for the repulsion between the ions. The introduction of the ZBL potential restricts the interatomic distances to realistic values. The four terms of the ZBL potential are important for different range of energies, but for  $K^+$  ions, with energies up to 200 KeV, which is much larger than the ones considered here, the interaction potential can be represented by a single term, which together with the Coulomb ionic part results in

$$U(r) = \frac{1}{r} + \frac{\alpha}{r} \exp\left(-\frac{r}{\rho}\right) \quad (22)$$

with  $\alpha = 184.1$  and  $\rho = 0.0569$  in scaled units, corresponding to 2650.6 eVÅ and 0.29529 Å, respectively in physical units. Figure 9 represents ZBL and Coulomb potentials, with their sum and other details to be commented later. Note that around  $r \simeq 0.4$ , the combined potential  $U(r)$  separates significantly from the Coulomb's potential.

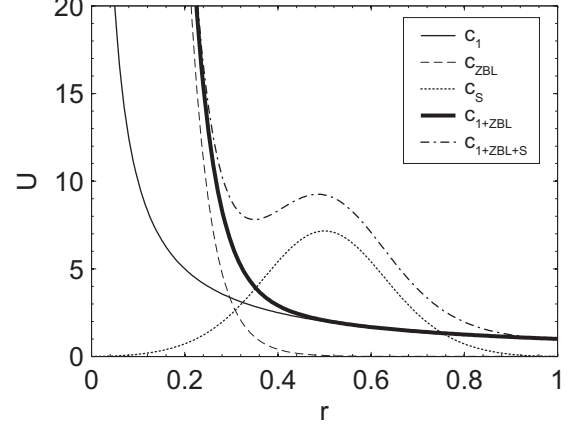


FIG. 9: Interaction potentials  $U(r)$  in scaled units. Coulomb ( $c_1$ ); ZBL ( $c_{\text{ZBL}}$ ); Coulomb+ZBL ( $c_{1+\text{ZBL}}$ ); substrate potential ( $c_s$ ) and the sum of Coulomb, ZBL and substrate potentials ( $c_{1+\text{ZBL}+s}$ ). The scaled units are 2.77 eV and the lattice unit  $a=5.19$  Å for  $U$  and  $r$  respectively.

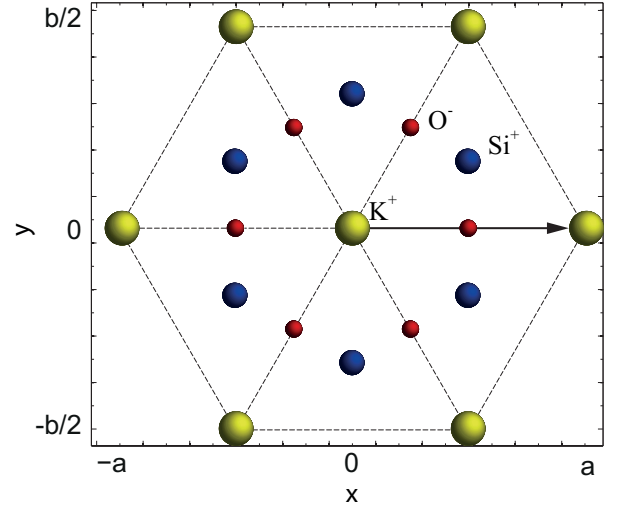


FIG. 10: Projection on the (001) plane of the ions used in the calculation of the substrate potential. Four planes of ions are considered, two above and two symmetrical below the  $K^+$  plane, the closest two with oxygen and the other two with silicon ions. The path for the central  $K^+$  ion used in the calculation is shown, note that the  $O^{-2}$  in the middle of the path are actually 1.68 Å, above and below. The interaction with the  $K^+$  ions in the same line (within a square) is not taken into account to calculate the substrate potential as it is used directly. The crystal is continued in the  $K^+$  plane until convergence is achieved. Distance between longer marks is 1 Å.

The dynamical equations become

$$\ddot{u}_n = -G_{n+1} + G_n - F_{n+1} + F_n, \quad (23)$$

with  $F_n$  given by Eq. (4) and  $G_n$  given by

$$G_n = \frac{\alpha}{1+v_n} \exp\left(-\frac{1+v_n}{\rho}\right) \left(\frac{1}{1+v_n} + \frac{1}{\rho}\right). \quad (24)$$

When the joint effect of both the screened Coulomb (ZBL) and bare Coulomb potentials is considered, i.e., Eq. (22), numerical simulations show that the behaviour of the kinks is not much different than that observed in the single bare Coulomb case, discussed in the preceding sections. Supersonic kinks propagate equally well, changing from the magic wavenumber to the proximity of  $q = \pi$  and also changing from sinusoidal to nearly triangular form. Figures 7 and 8 also show the characteristic curves  $V = V(A)$  and  $q = q(A)$ . The sound velocity does not change as the ZBL potential is felt only for very large perturbations. The RWA cannot be obtained analytically but the numerical RWA fits very well with the results of the simulations.

## V. THE EFFECT OF THE SUBSTRATE POTENTIAL: LATTICE KINKS OR CROWDIONS

In the preceding sections, the interaction with the other atoms in the crystal was taken into account only implicitly, since the effect of the surrounding atoms was to fix the lattice equilibrium distance and to confine the particles within the crystal. To better modelling the properties of kinks in a crystal as muscovite we take into account explicitly the interaction with the surrounding atoms in a simplified mica geometry. The  $K^+$  ions occupy the nodes of an hexagonal lattice with lattice unit 5.19 Å. There are not any other atoms in the  $K^+$  plane, therefore we need to consider more atoms above and below. We consider two planes above and two symmetric below. The closest plane, at a distance of 1.6795 Å is occupied with oxygen ions with charge -2, their projections on the  $K^+$  plane lie in the middle of the two nearest neighbours  $K^+$ . The other layers at a distance of 2.2227 Å from the  $K^+$  plane are occupied by silicon ions. They are in the centers of tetrahedra whose three horizontal vertices are occupied by the oxygen ions. See Fig. 10 for a sketch. The Si sites are occupied by  $Si^{+4}$  and  $Al^{+3}$  ions in a proportion of 3:1, giving an average charge of +3.75, but we assign them a smaller charge +2.75 to take into account other atoms in successive layers, particularly the oxygen ions at the top of the tetrahedra, and to achieve charge neutrality. We suppose that all atoms are in fixed positions except the moving  $K^+$  ions in a row in the [100] direction. This is justified because of the supersonic speed of the kinks, that we are interested in, and because of the weak interaction between ions compared to the ZBL interaction between potassium ions.

The interactions between  $K^+$  ions that are in the central  $X$ -axis are not considered to construct the substrate potential, as they are taken into account explicitly. The lattice is extended in the (001)  $K^+$  plane until convergence of the potential is achieved.

Specifically the potentials used are the electrostatic interactions and Born-Mayer potentials of the form  $V = A \exp(-r/r_g)$  given in Ref.<sup>24</sup>. The value of  $r_g = 0.29$  Å for all the interactions, and the pre-exponential con-

stants in eV are:  $A_{KO} = 3800.125$ ,  $A_{KSi} = 2762.5$ ,  $A_{OO} = 453.375$ ,  $A_{OSi} = 1851.25$ ,  $A_{SiSi} = 1173.125$ . For the  $K^+$ -interaction we use the ZBL potential described above.

We obtain a substrate potential in scaled units ( $u_E \simeq 2.77$  eV) which can be given with very good approximation by a truncated Fourier series:

$$U_s(x) = U_0 + \sum_{n=1}^4 U_n \cos(2\pi n x), \quad (25)$$

with coefficients  $U_n$  in  $\{2.4473, -3.3490, 1.0997, -0.2302, 0.0321\}$ . The corresponding linear frequency is  $\omega_0 = 4.48$  corresponding to 3.6 THz and  $119 \text{ cm}^{-1}$ , quite close to  $110 \text{ cm}^{-1}$  determined experimentally<sup>25</sup>. Also the potential well of 20 eV is coherent with molecular dynamics calculation<sup>26</sup>. It is represented in Fig. 9 together with the other potentials, so as their relative magnitudes can be compared.

The phonon spectrum becomes optical, the frequency and group velocity become

$$\begin{aligned} \omega^2 &= \omega_0^2 + 4c_s^2 \sin^2(q/2) \\ V_g &= \frac{d\omega}{dq} = \frac{c_s^2 \sin q}{\sqrt{\omega_0^2 + 4c_s^2 \sin^2(q/2)}}. \end{aligned} \quad (26)$$

Note that  $c_s$  is still the sound speed *without* substrate. The phonon frequencies  $\omega$  lie between  $\omega_0 = 4.48$  and  $\omega_{\max} = 5.31$ . The group velocity is zero at  $q = 0$  and  $q = \pi$  and has its maximum  $V_{g,\max} \simeq 0.4$  in the proximity of  $q = \pi/2$  with  $\lambda \simeq 4$ . These properties will be observed in the simulations.

### A. Qualitative description

The introduction of the substrate potential does not prevent supersonic lattice kinks to exist. The lattice kink, also called *crowdion*, consists of an interstitial propagating very fast in the lattice and leaving behind a vacancy. The specific feature of the kinks found in the present work is that its velocity and energy are fixed by the system, let us denote them as  $V_c$  and  $E_c$  ( $c$  for crowdion). If the energy given initially is smaller than  $E_c$  the kinks are rapidly dispersed and if it is larger the excess energy is radiated as the kink slows down to  $V_c$ . The specific values in scaled units are  $V_c = 2.7387 \simeq 2c_s$  and  $E_c = 9.4374$  corresponding to 7.16 km/s and 26.2 eV, respectively. The lattice kink is supersonic in two meanings a)  $V_c > c_s$ , where  $c_s$  is the sound velocity without substrate; b)  $V_c$  is much larger than the maximum phonon group speed  $V_{c,\max} \simeq 0.4$  in the system with substrate, but not larger than the maximum phase velocity which is unbounded as  $q \rightarrow 0$ .



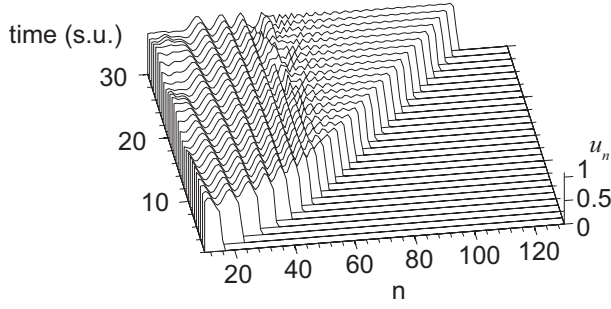


FIG. 11: Representation of the process of slowing down of the kink. The nonlinear and linear radiation processes can be easily distinguished. First, nonlinear waves with large amplitude are first emitted. Later, phonons with wavelength close to the maximum group velocity, with  $\lambda \simeq 4$ , and exponentially diminishing amplitudes while the kink approaches a limit velocity. Scaled time units are 0.2 ps, distances in lattice units.

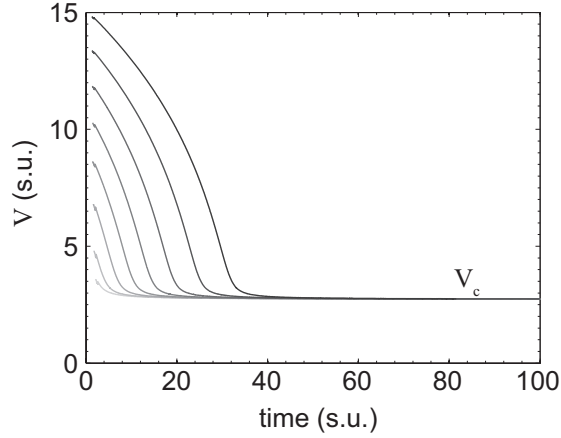


FIG. 12: Lattice kink or crowdion velocities with respect to time in scaled units for different initial conditions. For velocities  $V > V_c$  the lattice kink slows down until  $V = V_c$ . For  $V < V_c$  the kinks are dissipated into phonons. Scaled units are 0.2 ps and 2.6 km/s.

### B. Slowing down processes

The process of slowing down to  $V_c$  is shown in Figs. 11 and 12, two well distinguished phases can be identified.

a) *Nonlinear radiation:* For an initial energy  $E > E_c$ , the kink progressively loses energy. The particles immediately after the perturbation are left with enough energy to vibrate nonlinearly in the potential well bringing about nonlinear waves. Their frequencies obtained numerically are above the phonon band with maximum values of about 6.3. This strong radiative process is shown in Fig. 11 for an initial velocity  $V_0 = 7$ . This process is very fast and the loss of energy is almost linear with time.

b) *Linear radiation* As the lattice kink energy approaches to  $E_c$  the amplitude of the tail oscillations and its frequency decrease, entering into the phonon band,

therefore radiating low amplitude phonons<sup>16,17</sup>. The energy diminishes exponentially with time towards  $E_c$ . The wave number of the radiated phonons can be deduced from the kink speed as each particle left behind the kink is excited with a delay  $\Delta t = 1/V_c$  and, therefore, with a phase difference  $q = \omega(q)\Delta t = \omega(q)/V_c$ . As the phonon wavevector is given by  $q = \omega(q)/V_{ph}$ , where  $V_{ph}$  is the phase speed of the phonons,  $V_{ph} = V_c$ . Using the phonon dispersion relation in Eq. 26 it is possible to obtain the phonon wavenumber and wavelength  $\lambda_{ph} = 3.5$  which is the observed one in the simulations.

A similar process has been described in Ref.<sup>16</sup> and references therein for subsonic kinks. However, there is an important difference, the subsonic kinks described in those works radiate continuously and eventually stop.

### C. Double kink

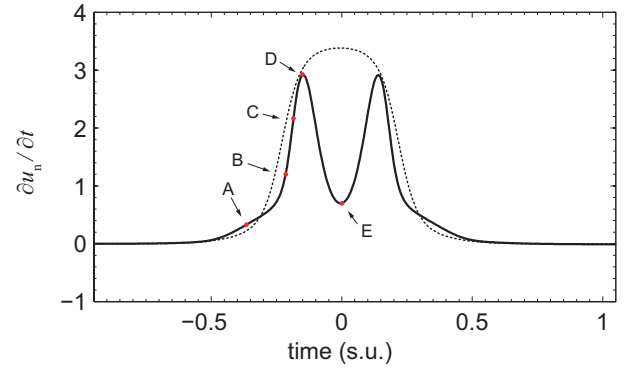


FIG. 13: Particle velocity waveform measured at  $n = 470$  and  $A = 0.67$  for Coulomb+ZBL potential without (dotted line) and with substrate potential (continuous line). The times when the ZBL interaction acts (near A) and the minimum velocity at the top of the potential barrier (E) are easily identified. The configurations at those times can be seen in Fig. 14. Scaled units are 0.2 ps and 2.6 km/s.

The particle velocity  $\dot{u}_n$  as a function of time for the stable kink is represented in Fig. 13. Due to the extreme discreteness of the kink it is not practical to represent  $\dot{u}_n$  as a function of  $n$ , while as a function of time the profile of a double soliton, corresponding to the double kink for the coordinates shown in Fig. 14(a) is evident.

Supersonic multi-solitons in Frenkel-Kontorova system with anharmonic coupling has been described in Refs. <sup>15,18,19</sup>. They correspond precisely to the discrete set of velocities for which the kinks do not radiate. Although roughly similar in shape the kink in our system do not correspond to the mathematical forms obtained in those references. It is more discrete, very close to the limit of discreteness, its wavenumber  $q \simeq 2\pi/3$  shown in Fig. 8 corresponds to only two particles moving at a given time.

This discreteness makes possible the exact description of the double kink process as shown in Fig. 14 (c): a particle  $n$ , represented as a white circle, initially at rest at

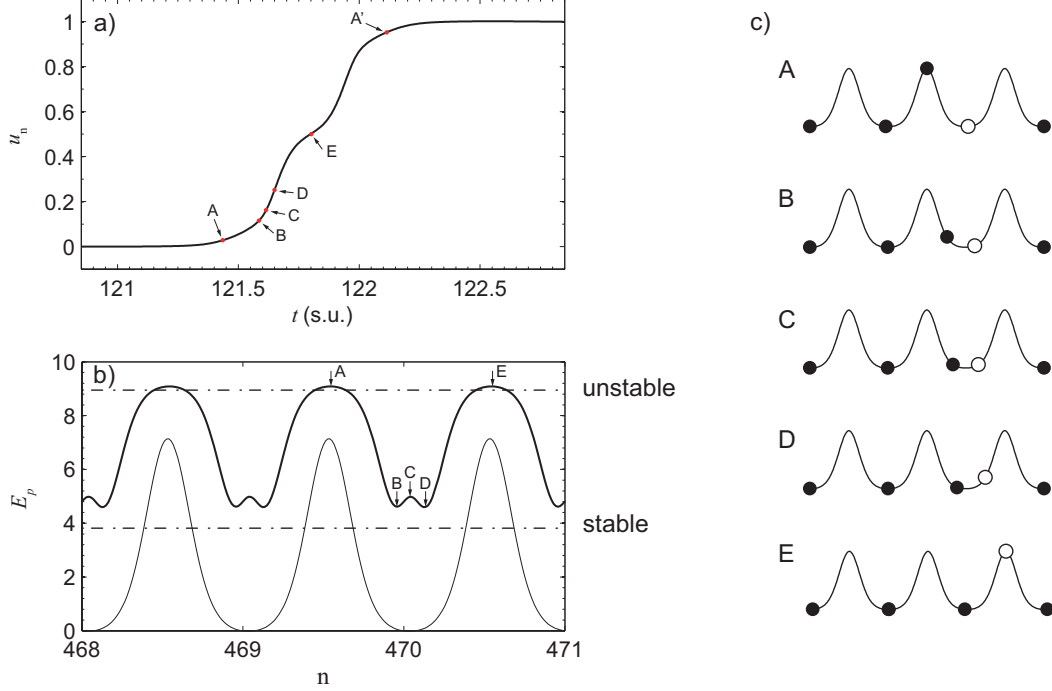


FIG. 14: (a) Particle displacement waveform for the established lattice kink, (b) Potential energy seen by the kink during propagation (thick line) and substrate periodic potential (thin line), horizontal lines are the energies corresponding to the equilibrium stable (C) and unstable (A) interstitial, (c) Particle configurations corresponding to the points A – F shown in (a) and (b). Scaled units are lattice unit for distances, 0.2 ps for time and 2.77 eV for energies.

the bottom of a potential well experiments two collisions, one when it is hit by the particle  $n - 1$  and accelerated, and a second when it hits the particle  $n + 1$  and is decelerated, attaining almost zero velocity at the bottom of the potential well (during the radiation process this velocity is different from zero). In between the two collisions, the particle finds the substrate potential barrier between sites and experiences a decrease in velocity when going uphill followed by an acceleration downhill.

Note that the states A and E in the same figure have exactly the same energy, but the kink has only moved half a lattice site. This is the first kink of the double-kink process shown in Fig. 14 (a). The process of the particle  $n$  going downhill and hitting particle  $n + 1$  until it stops forms the second kink.

The process can be seen in terms of the kink energy in Fig. 14 (b). Two identical oscillations of  $E_p$  happen for the kink to move a lattice site. There is a local maximum at point C corresponding to the minimum distance between particles and the short range ZBL interaction. The horizontal dashed-dotted lines indicate the energies for the equilibrium interstitial configurations, with two particles inside a potential well (stable), or one particle at the top of the potential barrier (unstable), their difference corresponding to the Peierls-Nabarro (PN) barrier. The potential energy is always above the stable interstitial energy as the lattice has no time to relax, bringing about an *adiabatic* PN barrier. The kink has always kinetic

energy, the minimum corresponding to configuration A.

## VI. CONCLUSIONS

In this paper we have modelled a low dimensional system using realistic potentials corresponding to a row of ions in a silicate layer, mica muscovite.

Our objective has been to determine if nonlinear localized modes existed with realistic parameters and with which characteristics. The choice of the parameters of mica muscovite is motivated by the fact that many of the dark tracks that appear in sheets of this material are consistent with in-layer propagation of vibrational excitations along close-packed lattice lines of ions, and an experiment has demonstrated that localized energy can travel along lattice directions, being able to eject an atom at the surface.

The modelling of the system has followed a process of increasing complexity to better understand which effect is due to which characteristic of the model. The starting model presented in a preliminary publication, was simply  $K^+$  ions with nearest neighbour Coulomb repulsion, for which we have found that very fast supersonic kinks propagate. They were extremely localized, only two or for higher energies almost a single particle is moving at the same time.

In the present paper we add analytical calculation of

the energies and compare them with simulations. We have also shown that the introduction of interaction with several neighbours do not produce significative changes as long as the sound speed in each system is taken as a reference. But the extremely short interatomic distances has motivated the introduction of a short range ZBL interaction. Again the changes are not important, kinks propagate equally well and with as much energy as desired, but now with realistic interatomic distances.

The following step has been the introduction of a substrate potential using empirical potentials and the geometry of the crystal. Supersonic kinks continue to propagate without losing energy but with several important properties: a) The main one is that the system selects exactly one velocity and one energy; b) The lattice kink energy is larger than the one needed for an atom ejection at the surface, and smaller than one of the proposed sources of energy, the recoil of a  $K^+$  ion due to beta emission; c) The kink can be described as double-kink or a bi-soliton depending of the variable chosen.

The extreme discreteness of the system with basically two particles moving at the same time allows for the detailed explanation of the double-kink, which was not possible in multi-kinks without dispersion presented in other works. It is produced by the matching of the two collisions experienced by a particle and the process of going over the potential barrier between sites.

We have shown that realistic potentials allow for the propagation of ultra discrete lattice kinks with energies that are consistent of properties observed in experiments. Although we cannot claim that those kinks are responsible for those phenomena it seems likely that they play a significant part.

### Acknowledgments

JFRA, VSM and LMGR acknowledge financial support from the projects FIS2008-04848, FIS2011-29731-C02-02 and MTM2012-36740-C02-02, from MICINN. All authors acknowledges Prof. FM Russell for continuous discussions.

### Appendix: Recoil energy of $^{40}\text{K}$

If the hypothesis of quodons being vibrational entities of ions of potassium is correct, the most likely source of energy is the recoil from  $^{40}\text{K}$  because a) the energy will be given directly to  $K^+$ , b) the relative abundance and decay frequency of  $^{40}\text{K}$ , and c) because of the energies involved as it is explained below.

The two most abundant isotopes are the stable  $^{39}\text{K}$  and  $^{41}\text{K}$ , with 93.7% and 6.7% abundance respectively. The following is  $^{40}\text{K}$  with a very long half life of  $1.248 \times 10^9$  years and abundance 0.0117%. This isotope is the most important source of radioactivity for humans.

$^{40}\text{K}$  experiments decay through different branches with two daughter nuclei  $^{40}\text{Ca}$  and  $^{40}\text{Ar}$ <sup>27,28</sup>, the main parameters of the decay are  $I$ , the intensity of a given branch in % and  $Q$ , which is the difference between the rest mass of the parent nucleus and the rest masses of the daughter particles, which can be an electron or positron and a neutrino and the daughter nucleus.  $Q$  is also the kinetic energy available for the daughter particles plus the possible photon energies.

Some of the decay branches,  $\beta^-$  and  $\beta^+$  involve the emission of an electron or a positron and a neutrino. The electron or positron velocities are such that they have to be treated relativistically, while the recoil velocity of the much heavier nuclei can be described classically. We will suppose an electron to simplify the language, but it can be equally a positron in what follows. The neutrino can be considered a massless particle as the rest mass it known to be below  $2.2 \text{ eV}/c^2$ . The maximum recoil energy is obtained when the neutrino gets no kinetic energy. The recoil energy is much smaller than the electron energy, so it can be neglected in the calculations. The electron maximum energy is  $E = m_e c^2 + Q$ , with  $E^2 = m_e^2 c^4 + p_e^2 c^2$ ,  $p_e$  being the momentum of the electron. Considering the parent nucleus at rest, the momentum of the nucleus is identical to the momentum of the electron  $p_N = p_e = (1/c)(E^2 - m_e^2 c^4)^{1/2}$  and the maximum nucleus recoil energy is given by  $E_k = p_N^2 / (2m_N)$ . A secondary process that may occur in the  $^{40}\text{K}$  decay is the emission of a gamma photon, in this case the recoil momentum is equal to energy of the gamma photon  $p_N = p_\gamma$  and trivially  $E_N = P_N^2 / (2m_N)$ . In this case, the energy  $E_N$  is a single value and not the maximum.

Other data of interest are the ionization energies of K and of the daughter nuclei. If the recoil energy is larger than the ionization energy of the first electrons, it can be used to ionize an atom or ion and the energy cannot be transferred to the neighbours. The first ionization energies for K are 4.34 and 31.6 eV, for Ar 15.8 and 27.6 eV and for  $^{40}\text{Ca}$  are 6.1, 11.9 and 50.6 eV<sup>29</sup>. It is therefore probable that 31.6 eV is an upper limit for crowdion energy in a  $K^+$  lattice.

### $^{40}\text{K}$ decay branches

The  $^{40}\text{K}$  decay branch that leads to  $^{40}\text{Ca}$  is:

$\beta^-$  decay: with  $I\beta^- = 89.25\%$  and  $Q = 1311.07 \text{ keV}$ . The maximum kinetic energy of the electron or *endpoint* is almost equal to  $Q$ . The daughter nuclei of  $^{40}\text{Ca}$  have a continuous distribution of energy with a maximum of  $T = 42 \text{ eV}$  at the endpoint corresponding to a velocity  $V = 16 \text{ km/s}$ .

The proton number increases in one, but the number of electrons does not change, therefore the daughter ion would be  $\text{Ca}^{++}$  with 50.6 eV third ionization energy. This is a likely origin of quodons for the decays with recoil energy smaller than

31.6 eV.

The following processes have  $^{40}\text{Ar}$  as daughter nuclei

*Electron capture and  $\gamma$  radiation*,  $I\epsilon = 10.55\%$ . First, and electron from the shell is captured leading to an excited nucleus of  $^{40}\text{Ar}^+$ , which decays to the ground state with the emission of a  $\gamma$  ray of 1460.82 keV. The corresponding recoil energy of  $^{40}\text{Ar}$  is  $T \simeq 29$  eV with velocity  $V = 12.0$  km/s. As this is a two body process  $T$  has only slight variations due to interactions with the shell electrons.

As no charge is emitted from the ion  $\text{K}^+$ , the daughter will be also a monovalent ion of  $\text{Ar}^+$ , with 27.7 eV second ionization energy. So there is some probability that the  $\text{Ar}$  collision with  $\text{K}^+$  will lead to the second ionization of  $\text{Ar}$ .

*Electron capture and decay to the ground state*: with  $I = 0.2\%$ , this process is usually attributed to a conversion electron process. That is, a shell electron takes most of the available energy  $Q = 1505.60$  keV minus the electron binding energy which is at most a few keV. This is also a two body process with almost fixed recoil energy  $T \simeq 52$  eV ( $V = 16$  km/s).

The daughter nucleus has lost a proton but also the shell has lost an electron, therefore the daughter ion will be  $\text{Ar}^+$  with second ionization energy of 27.7 eV, so there is a high probability that either an ion of  $\text{K}^+$  or  $\text{Ar}^+$  could be ionized in the first collision, but then the remaining energy may be enough to produce a quodon.

$\beta^+$  decay, with very low probability  $I\beta^+ = 0.001\%$  and  $Q = 482.9$ . The energy  $Q$  is shared between the neutrino, the emitted positron and the daughter nucleus. Therefore, the latter have a continuum of recoil energies with maximum kinetic energy  $T \simeq 10$  eV.

As the proton number is decreased in one unit,  $Z-1$  but there is no change in the number of electrons, the daughter ion will be a neutral  $\text{Ar}$  interacting with short range forces with the neighbouring  $\text{K}^+$ . The first ionization energy of  $\text{Ar}$  is 15.8 eV and the second 27.7 eV, so, actually, the  $\text{Ar}$  atom has not enough energy for ionizing nor for the second ionization of  $\text{K}^+$ .

## Secondary processes

*Electron-positron pair production* This is secondary process after the  $\gamma$  ray emission of 1460.82 keV considered above. It needs the interaction of the  $\gamma$  ray with a nucleus, and the produced positron and electron can share the energy in any proportion. The maximum recoil energy corresponds to a single particle taking almost all the energy except for the small amount taken by the nucleus, which is necessary due to momentum conservation. The kinetic energy available is  $Q = E_\gamma - 2m_e c^2 = 437.4$  keV and the maximum recoil energy is  $T = 8.8$  eV. The probability of the combined process of electron capture and pair production is of the same order of magnitude to the  $\beta^+$  emission and also the energies<sup>30</sup>. The probability of interaction of the  $\gamma$  ray with a nucleus is proportional to  $Z^2$  which favors the interaction with potassium, however, they are only 5% of the atoms in mica.

As the energy is smaller than the second ionization energy of potassium 31.7 eV it is likely that the subsequent  $\text{K}^+ - \text{K}^+$  collisions are elastic.

Other secondary processes may occur also from the presence of other radioactive nuclei and the corresponding decay, but it will be beyond the objective of this work to continue the subject further.

<sup>1</sup> S. A. Durrani. Nuclear tracks: A success story of the 20th century. *Rad. Meas.*, 34:5–13, 2001.

<sup>2</sup> S. A. Durrani. Nuclear tracks today: Strengths, weaknesses, challenges. *Rad. Meas.*, 43:S26–S33, 2008.

<sup>3</sup> F. M. Russell. Tracks in mica caused by electron showers. *Nature*, 216:907–909, 1967.

<sup>4</sup> F. M. Russell. Duration of sensitive period for track recording in mica. *Nature*, 217:51–52, 1967.

<sup>5</sup> F. M. Russell. Positive charge transport in layered crystalline solids. *Phys. Lett. A*, 130:489–491, 1988.

<sup>6</sup> F. Russell. Identification and selection criteria for charged lepton tracks in mica. *Nucl. Tracks. Rad. Meas.*, 15:41–44, 1988.

<sup>7</sup> D. Schler, K. Kroneberger, M. Schosnig, F. M. Russell, and K. O. Groeneveld. Search for solitons in solids. *Rad. Meas.*, 23:209–213, 1994.

<sup>8</sup> F. M. Russell and J. C. Eilbeck. Evidence for moving

breathers in a layered crystal insulator at 300K. *Europhys. Lett.*, 78:10004, 2007.

<sup>9</sup> Y. Kudriavtsev, A. Villegas, A. Godines, and R. Asomoza. Calculation of the surface binding energy for ion sputtered particles. *Appl. Surf. Sci.*, 239(3–4):273–278, 2005.

<sup>10</sup> Q. Dou, J. Cuevas, J. C. Eilbeck, and F. M. Russell. Breathers and kinks in a simulated crystal experiment. *Discret. Contin. Dyn. S.-S*, 4:1107–1118, 2011.

<sup>11</sup> J. F. R. Archilla, Yu. Kosevich, N. Jiménez, V. Sánchez-Morcillo, and L. M. García-Raffi. Moving excitations in cation lattices. *Ucr. J. Phys.*, 58(7):646–656, 2013.

<sup>12</sup> J.F.R. Archilla, Y. A. Kosevich, N. Jiménez, V.J. Sánchez-Morcillo, and L.M. García-Raffi. Supersonic kinks in Coulomb lattices. In R. Carretero et al, editor, *Localized Excitations in Nonlinear Complex Systems*, pages 317–331. Springer, 2014.

<sup>13</sup> J. Biersack, J.P. Ziegler, and M.D. Ziegler. *SRIM - The*

- Stopping and Range of Ions in Matter*. Published by J.P. Ziegler, 2008.
- <sup>14</sup> A. V. Savin and Yu A. Kosevich. Thermal conductivity of molecular chains with asymmetric potentials of pair interactions. *Phys. Rev. E*, 89:032102, 2014.
  - <sup>15</sup> A.M. Kosevich and A.S. Kovalev. The supersonic motion of a crowdion. The one dimensional model with nonlinear interaction between the nearest neighbors. *Solid State Commun.*, 12:763–764, 1973.
  - <sup>16</sup> O M Braun and Yu S Kivshar. Nonlinear dynamics of the Frenkel–Kontorova model. *Phys. Rep.*, 306:1–108, 1998.
  - <sup>17</sup> Yu.S. Kivshar O.M. Braun. *The Frenkel-Kontorova Model*. Springer, 2004.
  - <sup>18</sup> A.V. Savin. Supersonic regimes of motion of a topological soliton. *Sov. Phys. JETP*, 81:608–613, 1995.
  - <sup>19</sup> Y. Zolotaryuk, J.C Eilbeck, and A.V. Savin. Bound states of lattice solitons and their bifurcations. *Physica D*, 108:81–91, 1997.
  - <sup>20</sup> Y Ni, Yu A. Kosevich, S. Xiong, Y. Chalopin, and S. Volz. Substrate-induced cross-plane thermal propagative modes in few-layer graphene. *Phys. Rev. B*, 89:205413, 2014.
  - <sup>21</sup> Yu. A. Kosevich, R. Khomeriki, and S. Ruffo. Supersonic discrete kink-solitons and sinusoidal patterns with magic wave number in anharmonic lattices. *Europhys. Lett.*, 66:21–27, 2004.
  - <sup>22</sup> G. Friesecke and K. Matthies. Atomic-scale localization of high-energy solitary waves on lattices. *Physica D*, 171(4):211 – 220, 2002.
  - <sup>23</sup> M. Molerón, A. Leonard, and C. Daraio. Solitary waves in a chain of repelling magnets. *J. Appl. Phys.*, 115(18):184901, 2014.
  - <sup>24</sup> O. Gedeon, J. Machacek, and M. Liska. Static energy hypersurface mapping of potassium cations in potassium silicate glasses. *Phys. Chem. Glass.*, 43(5):241–246, 2002.
  - <sup>25</sup> M Diaz, V. C. Farmer, and R Prost. Characterization and assignment of far infrared absorption bands of  $K^+$  in muscovite. *Clays Clay Miner.*, 48:433–438, 2000.
  - <sup>26</sup> D R Collins and C R A Catlow. Computer simulation of structure and cohesive properties of micas. *Am. Min.*, 77:1172–1181, 1992.
  - <sup>27</sup> JA Cameron and B Singh. Nuclear data sheets for a=40. *Nucl. Data Sheets*, 102(2):293–513, 2004.
  - <sup>28</sup> X. Mougeot and R. G. Helmer. LNE-LNHB/CEA–Table de Radionuclides, K-40 tables. <http://www.nucleide.org>, 2012.
  - <sup>29</sup> D. R. Lide, editor. *Handbook of Chemistry and Physics*. CRC Press, Boca Raton, Florida, USA, 90<sup>th</sup> edition, 2010. Section 10, page 203.
  - <sup>30</sup> D. W. Engelkemeir, K. F. Flynn, and L. E. Glendenin. Positron emission in the decay of  $K^{40}$ . *Phys. Rev.*, 126(5):1818–1822, 1962.